Ensemble Simulations of a Nonlinear Barotropic Model for the North Atlantic Oscillation

ZHANG Dong-Bin[1,2], JIN Fei-Fei[3], LI Jian-Ping[1], and DING Rui-Qiang[1]

[1] State Key Laboratory of Numerical Modeling for Atmospheric Sciences and Geophysical Fluid Dynamics (LASG), Institute of Atmospheric Physics, Chinese Academy of Sciences, Beijing 100029, China
[2] Graduate University of Chinese Academy of Sciences, Beijing 100049, China
[3] Department of Meteorology, University of Hawaii at Manoa, Honolulu, Hi 96822, USA

Abstract   A numerical ensemble-mean approach was employed to solve a nonlinear barotropic model with stochastic basic flows to analyze the nonlinear effects in the formation of the North Atlantic Oscillation (NAO). The nonlinear response to external forcing was more similar to the NAO mode than the linear response was, indicating the importance of nonlinearity. With increasing external forcing and enhanced low-frequency anomalies, the effect of nonlinearity increased. Therefore, for strong NAO events, nonlinearity should be considered.

Keywords: ensemble-mean, NAO, nonlinearity

Citation: Zhang, D.-B., F.-F. Jin, J.-P. Li, et al., 2010: Ensemble simulations of a nonlinear barotropic model for the North Atlantic Oscillation, *Atmos. Oceanic Sci. Lett.*, **3**, 277–282.

1   Introduction

The North Atlantic Oscillation (NAO) is a prominent mode of the general atmospheric circulation in the Northern Hemisphere during the winter (Walker and Bliss, 1932; Wallace and Gutzler, 1981) and can be considered part of the global-scale northern annular mode (NAM) (Thompson and Wallace, 1998, 2000; Li and Wang, 2003a, b). The NAO represents some of the important characteristics of low-frequency variability in general circulation, and it may influence precipitation, ecology, and aquaculture in Europe (Hurrell et al., 2003) as well as the East Asian monsoon and related precipitation events (Wu and Huang, 1999; Zhou et al., 2000; Fu and Zeng, 2005; Wu et al., 2009).

Many factors may bring on the NAO, including external forcing (e.g., sea surface temperature anomalies, sea ice, and snow cover) (Watanabe and Nitta, 1998, 1999; Wu et al., 2000), the instability of basic flow (Simmons et al., 1983; Branstator, 1992), and the interaction between eddies and low-frequency flow (Lau, 1988; Cai and Mak, 1990; Branstator, 1995). Previous studies have suggested that intrinsic atmospheric processes have important roles in causing and maintaining the NAO, and the so-called "transient eddy forcing" concept has been proposed as a mechanism that underlies the NAO (Kug and Jin, 2009; Kug et al., 2009).

In the present study, we focused on nonlinear intrinsic processes that contribute to the excitation of an NAO-like

Corresponding author: ZHANG Dong-Bin, zdb@mail.iap.ac.cn

response. To consider the effect of transient eddies on low-frequency anomalies, we used a nonlinear barotropic model with stochastic basic flows.

2   Data

We analyzed 30 years of daily 500-hPa streamfunction data ψ (December–February, 1979/80–2008/09) derived from the National Centers for Environmental Prediction-National Center for Atmospheric Research (NCEP-NCAR) reanalysis (Kalnay et al., 1996). To obtain the high-frequency component of ψ (i.e., ψ', the transient synoptic eddy flow), daily data with the monthly mean subtracted were band-pass filtered over the period of 2.5–8.0 days (Murakami, 1979). The NAO index was obtained from the website of the Climate Prediction Center of the USA (http://www.cpc.ncep.noaa.gov/data/tele-doc/telecontents.shtml).

3   Barotropic model with a stochastic basic flow

The streamfunction ψ can be decomposed to $\psi = \overline{\psi}^c + \overline{\psi}^a + \psi'$, where $\overline{\psi}^c$ is the climatological mean, $\overline{\psi}^a$ is the low-frequency anomaly, and ψ' is the high-frequency component, representing the transient eddy flow.

Using the above decomposition, based on the following barotropic equation

$$\frac{\partial}{\partial t}\Delta\psi + J(\psi, \Delta\psi + f) + r\Delta\psi = Q , \qquad (1)$$

where f is the Coriolis parameter, r is the diffusion coefficient, Q is the external forcing, and J is the Jacobian operator. The equation for $\overline{\psi}^a$ can be written as

$$\frac{\partial}{\partial t}\Delta\overline{\psi}^a + L\overline{\psi}^a + r\Delta\overline{\psi}^a + J(\overline{\psi}^a, \Delta\overline{\psi}^a) + \overline{J(\psi', \Delta\psi')}^a = \overline{Q}^a ,$$

$$(2)$$

where L is the linear operator, and $L\overline{\psi}^a = J(\overline{\psi}^c, \Delta\overline{\psi}^a) + J(\overline{\psi}^a, \Delta\overline{\psi}^c + f)$.

The term $\overline{J(\psi', \Delta\psi')}^a$ represents the transient eddy forcing. Jin et al. (2006a, b) developed a new approach for reconstructing this term using historical observed data, adopting the view that the evolution of atmospheric circulation is a particular realization of a hypothetical sto-

chastic flow ensemble, which is denoted as Ψ. Ψ can be decomposed as $\Psi = \Psi_c + \Psi_a$, where Ψ_c and Ψ_a represent the basic and anomalous ensembles of the stochastic flow, respectively. Each of these three terms is further decomposed into its ensemble mean (denoted by the $<\ >$ term) and the deviation (denoted by the prime term):

$$\Psi_c = <\Psi_c> + \Psi_c', \quad \Psi_a = <\Psi_a> + \Psi_a', \text{ and } \Psi = <\Psi> + \Psi'.$$

Under the ergodic approximation, $<\Psi_c> \approx \overline{\psi}^c$ and $<\Psi_a> \approx \overline{\psi}^a$. Therefore, ψ' can be viewed as a particular realization of Ψ'.

Assuming that Ψ also follows the barotropic equation, we obtained a barotropic model with stochastic basic flows:

$$\frac{\partial}{\partial t}\Delta\Psi_a + L\Psi_a + J(\Psi_c', \Delta\Psi_a) + J(\Psi_a, \Delta\Psi_c')$$
$$+ r\Delta\Psi_a + J(\Psi_a, \Delta\Psi_a) = Q_a . \quad (3)$$

Jin and Lin (2007) proposed an approach involving numerical ensemble-mean simulations to solve the linear version of the model. Using this approach, the stochastic basic flow is

$$\Psi_c' = \sum_{n=1}^{N_c} \sigma_n \xi_n(t) E_n(\lambda, \varphi) e^{i\omega_n t} + cc , \quad (4)$$

here, λ is the longitude, and φ is the latitude. The variance contribution σ_n, the CEOF spatial mode E_n, and the frequency of each mode ω_n can be derived from a complex empirical orthogonal function (CEOF) analysis of the observed transient eddy flow ψ' (for details, see Jin et al., 2006a). N_c is the number of CEOF modes. $\xi_n(t)$ is an independent Gaussian red-noise process, as follows:

$$\frac{d\xi_n}{dt} = -\xi_n / \tau_n + w_n(t) , \quad (5)$$

where $w_n(t)$ represents complex normalized white noise, and τ_n is the e-folding time of a transient eddy.

The numerical ensemble-mean approach first generates normalized Gaussian random variables for $w_n(t)$ and then integrates Eq. (5) to obtain $\xi_n(t)$. By choosing 200 sets of random number sequences, we generated 200 members of the realization for each $\xi_n(t)$, and furthermore, we obtained 200 members of the realization for the stochastic basic flow Ψ_c'. For each realization of Ψ_c', we can obtain Ψ_a by solving Eq. (3), thereby obtaining the ensemble-mean of the solutions $<\Psi_a>$, which is the approximation of the low-frequency anomaly $<\Psi_a> \approx \overline{\psi}^a$.

The ensemble mean of Eq. (3) is

$$\frac{\partial}{\partial t}\Delta<\Psi_a> + L<\Psi_a> + r\Delta<\Psi_a>$$
$$+ [<J(\Psi_c', \Delta\Psi_a')> + <J(\Psi_a', \Delta\Psi_c')>]$$
$$+ [J(<\Psi_a>, \Delta<\Psi_a>) + <J(\Psi_a', \Delta\Psi_a')>] = <Q_a> . \quad (6)$$

The term $J(<\Psi_a>, \Delta<\Psi_a>)$ is a deterministic nonlinear tendency, the term $<J(\Psi_c', \Delta\Psi_a')> + <J(\Psi_a', \Delta\Psi_c')>$ is a stochastic-eddy-induced linear tendency, and $<J(\Psi_a', \Delta\Psi_a')>$ is a stochastic-eddy-induced nonlinear tendency.

Thus,

$$\overline{J(\psi', \Delta\psi')}^a \approx <J(\Psi_c', \Delta\Psi_a)> + <J(\Psi_a, \Delta\Psi_c')>$$
$$+ <J(\Psi_a', \Delta\Psi_a')> .$$

$J(<\Psi_a>, \Delta<\Psi_a>)$ and $<J(\Psi_a', \Delta\Psi_a')>$ are two major sources of nonlinearity in the barotropic model. Here, we used the numerical ensemble-mean approach to solve the linear and nonlinear models separately to analyze the contribution of nonlinear terms to the formation of the NAO mode.

4 Results

4.1 External forcing of the NAO

Using the observed data, we calculated the external forcing of the NAO. The NAO mode was obtained by regressing the monthly anomalous streamfunction onto the NAO index, denoted as NAO^{reg}. Letting $\overline{\psi}^a$ = NAO^{reg}, the external forcing is as follows:

$$\overline{Q}^a = L\overline{\psi}^a + r\Delta\overline{\psi}^a + J(\overline{\psi}^a, \Delta\overline{\psi}^a) + \overline{J(\psi', \Delta\psi')}^a ,$$

where $\overline{J(\psi', \Delta\psi')}^a$ is obtained by regressing $J(\psi', \Delta\psi')$ onto the NAO index.

The stream fields of each term in the external forcing are shown in Fig. 1. The effect of climatological mean flow is dominant, although we cannot ignore the interaction between the eddy and low-frequency flow or the deterministic nonlinear tendency. The tendency $J(<\Psi_a>, \Delta<\Psi_a>)$, which is determined by the low-frequency anomaly, reflects the nonlinear characteristics of the NAO mode.

4.2 Differences between the linear and nonlinear solutions

We solved the linear and nonlinear equations that included the external forcing $\overline{Q}^a$. We compared the results of the linear and nonlinear adjustment processes to external forcing to explore the contribution of nonlinearity to the formation of the NAO.

The numerical results are shown in Fig. 2. The nonlinear response (Fig. 2c) approached the NAO mode to a greater degree than did the linear response (Fig. 2b).

We defined the relative difference between two fields as follows:

$$rd = \frac{\sqrt{\int |var - var_0|^2 \, dx \, dy}}{\sqrt{\int |var_0|^2 \, dx \, dy}} ,$$

where var_0 is the reference field, and $var - var_0$ is the difference field. The ratio of the square roots of these terms for a given region (the Northern Hemisphere in this case) represents the relative difference between var and var_0.

The relative differences between each of the two responses and the NAO were 0.32 (linear) and 0.15 (nonlinear), suggesting that the response is more similar to the NAO when nonlinear terms are considered. This finding indicates that the nonlinear effect is important in
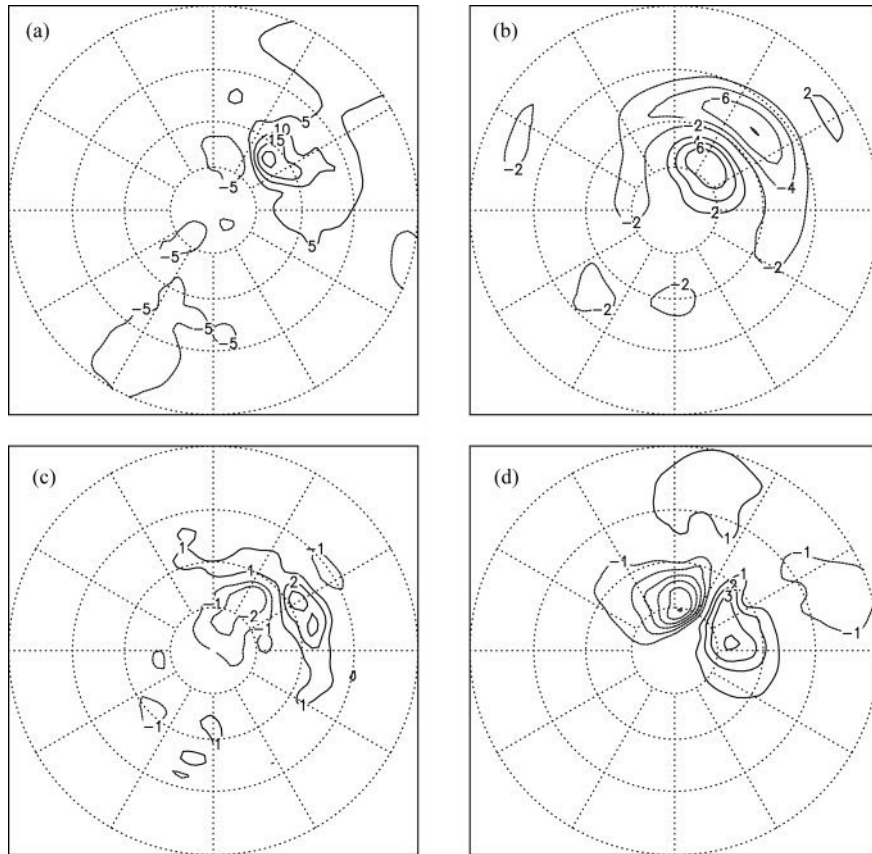
Figure 1 Diagnostic forcing (based on NCEP-NCAR reanalysis data from December to February, 1979/80–2008/09) for (a) $-\Delta^{-1}L\bar{\psi}^a$, (b) $-r\bar{\psi}^a$, (c) $-\Delta^{-1}\overline{J(\psi',\Delta\psi')}^a$, and (d) $-\Delta^{-1}J(\bar{\psi}^a,\Delta\bar{\psi}^a)$ (Units: $m^2 s^{-2}$).
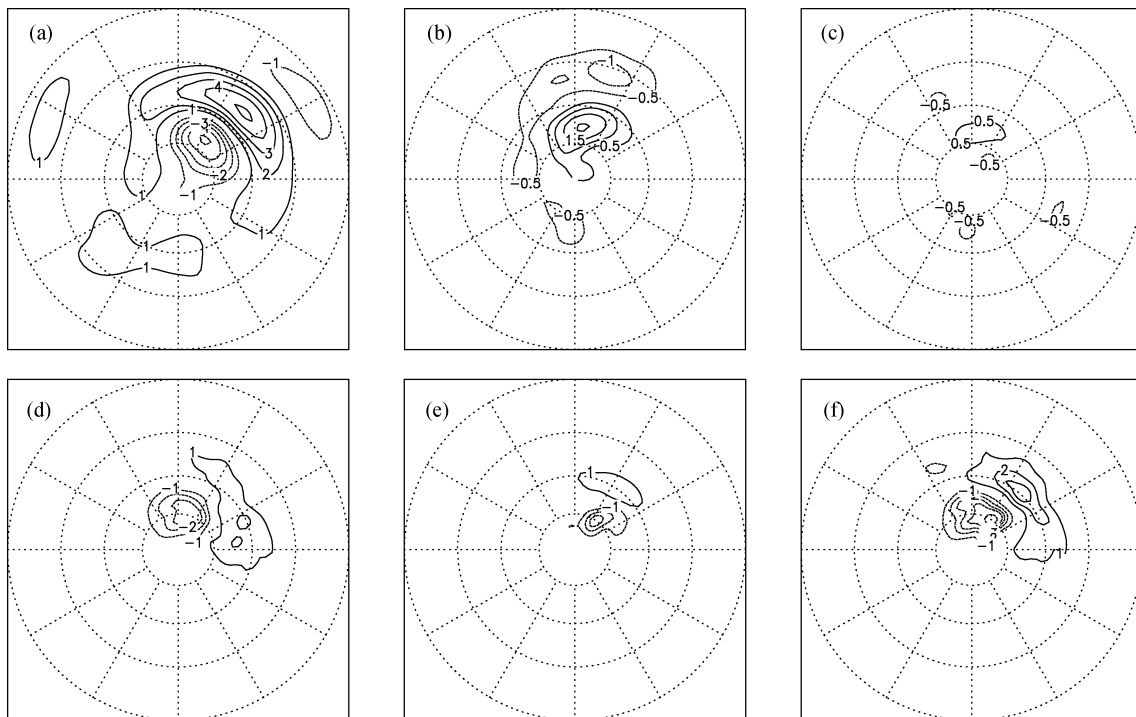

Figure 2 Steady responses and eddy forcing. (a) Regression NAO mode; (b) Difference field between the linear response and the NAO mode; (c) Same as (b), but for a nonlinear response; (d) Linear eddy forcing, $-\Delta^{-1}[<J(\Psi_a',\Delta\Psi_c')>+<J(\Psi_c',\Delta\Psi_a')>]$; (e) Nonlinear eddy forcing, $-\Delta^{-1}<J(\Psi_a',\Delta\Psi_a')>$; (f) Total eddy forcing. The units in (a)–(c) are $10^6\ m^2 s^{-2}$; those in (d)–(f) are $m^2 s^{-2}$.

the excitation of the NAO.

The stochastic-eddy-induced nonlinear tendency $<J(\Psi_a',\Delta\Psi_a')>$ has the same magnitude as the linear tendency $<J(\Psi_a',\Delta\Psi_c')>+<J(\Psi_c',\Delta\Psi_a')>$. When the nonlinear component was considered (compared with the linear component), the eddy forcing was more similar to the $\overline{J(\psi',\Delta\psi')}^a$ derived from observation. This result suggests that the nonlinear model is more accurate than the linear model in describing the interaction between eddies and low-frequency flow.

4.3   Results of ideal experiments

The results in Section 4.2 suggest that nonlinearity makes a considerable contribution to the formation of the NAO. The NAO mode has a certain nonlinear characteristic in that its spatial pattern and intensity result in a relatively large nonlinear tendency $J(\overline{\psi}^a,\Delta\overline{\psi}^a)$. The response of the atmosphere depends on external forcing. Briefly, an increase in the forcing amplitude corresponds to an increase in the response (low-frequency anomaly) amplitude, as well as an increase in $J(\overline{\psi}^a,\Delta\overline{\psi}^a)$.

We next considered the effect of nonlinearity by multiplying the coefficient α by the external forcing and calculating the relative difference between the linear and nonlinear solutions. Figure 3 shows the variability in the relative difference as a function of the coefficient α, revealing that the effect of nonlinearity increases with increasing forcing amplitude.

4.4   Results from observed data

The results in Section 4.3 are from ideal experiments. We also analyzed the dependence of the nonlinear effect on external forcing and low-frequency anomalies using observed data. We analyzed the positive and negative NAO phases during the winters from 1979/80 to 2008/09. Based on a composite analysis, we obtained the positive phase mode (NAO$^+$) and the negative phase mode
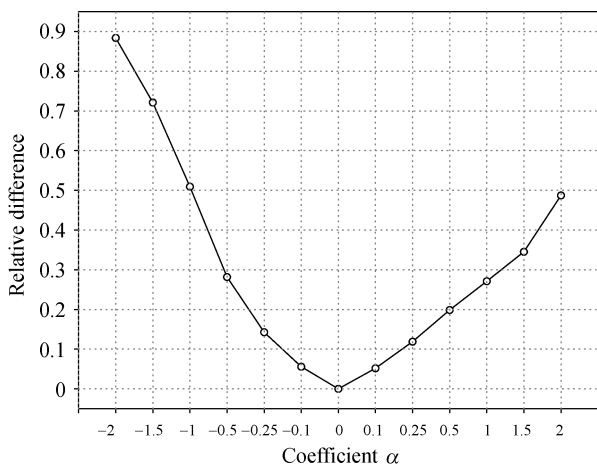

Figure 3   Relative difference between the linear and nonlinear solutions.

(NAO$^-$), and we calculated the corresponding eddy forcing $\overline{J(\psi',\Delta\psi')}^a$.

Letting $\overline{\psi}^a = \text{NAO}^+$ and $\overline{\psi}^a = \text{NAO}^-$, we obtained the corresponding external forcing and then solved the linear and nonlinear models; the solutions are shown in Fig. 4. The nonlinear solutions were more similar to the NAO mode than were the linear solutions, which is consistent with the result obtained using NAO^{reg}.

Table 1 lists the relative differences among the three cases (which correspond to NAO^{reg}, NAO$^+$, and NAO$^-$). The amplitudes and external forcings of NAO$^+$ and NAO$^-$ were larger than those of NAP^{reg}. Thus, the relative differences between the linear and nonlinear solutions from NAP$^+$ and NAO$^-$ were larger than the result for NAO^{reg}. The findings from the observed data also suggest that increased external forcing and enhanced low-frequency anomalies are associated with an increasing effect of nonlinearity.

To compare the results obtained from the observed data with those obtained from the ideal experiments, we made the following simplifications. NAO^{reg} is denoted as $\overline{\psi}^0$, and its corresponding external forcing is

$$\overline{Q}^0 = L\overline{\psi}^0 + r\Delta\overline{\psi}^0 + J(\overline{\psi}^0,\Delta\overline{\psi}^0) + \overline{J(\psi',\Delta\psi')}^a.$$

Because the composite NAO modes have similar spatial patterns to NAO^{reg}, they can be approximately denoted as $\lambda \times \overline{\psi}^0$. Thus, we have

$$\overline{Q}^a = \lambda \times L\overline{\psi}^0 + \lambda \times r\Delta\overline{\psi}^0 + \lambda^2 \\ \times J(\overline{\psi}^0,\Delta\overline{\psi}^0) + \overline{J(\psi',\Delta\psi')}^a.$$

The difference fields of $\overline{J(\psi',\Delta\psi')}^a$ in the three cases (which correspond to NAO^{reg}, NAO$^+$, and NAO$^-$ respectively) are small relative to other terms. We use δ to denote a small positive value. For NAO$^+$, $\lambda \approx 2-\delta$; consequently, $\overline{Q}^a \approx 2 \times \overline{Q}^0 + \delta$. The value of the relative difference rd (0.54) was slightly larger than the value of rd (α=2) (0.49) obtained from ideal experiments. For NAO$^-$, $\lambda \approx -2+\delta$; consequently, $|\overline{Q}^a| < 2 \times |\overline{Q}^0|$. In the ideal experiments, the value of rd (0.75) was smaller than the value of rd (α=−2) (0.88). Therefore, the results obtained from the observed data are consistent with the results from the ideal experiments.

5   Conclusion

We used an ensemble-mean approach to solve linear and nonlinear barotropic models with stochastic basic flows, and we analyzed the contribution of nonlinearity in the formation of the NAO. The analysis yielded the following results.

(1) Transient eddy forcing contains linear and nonlinear components. The nonlinear model was more accurate than the linear model in depicting the interaction between eddies and low-frequency flow.
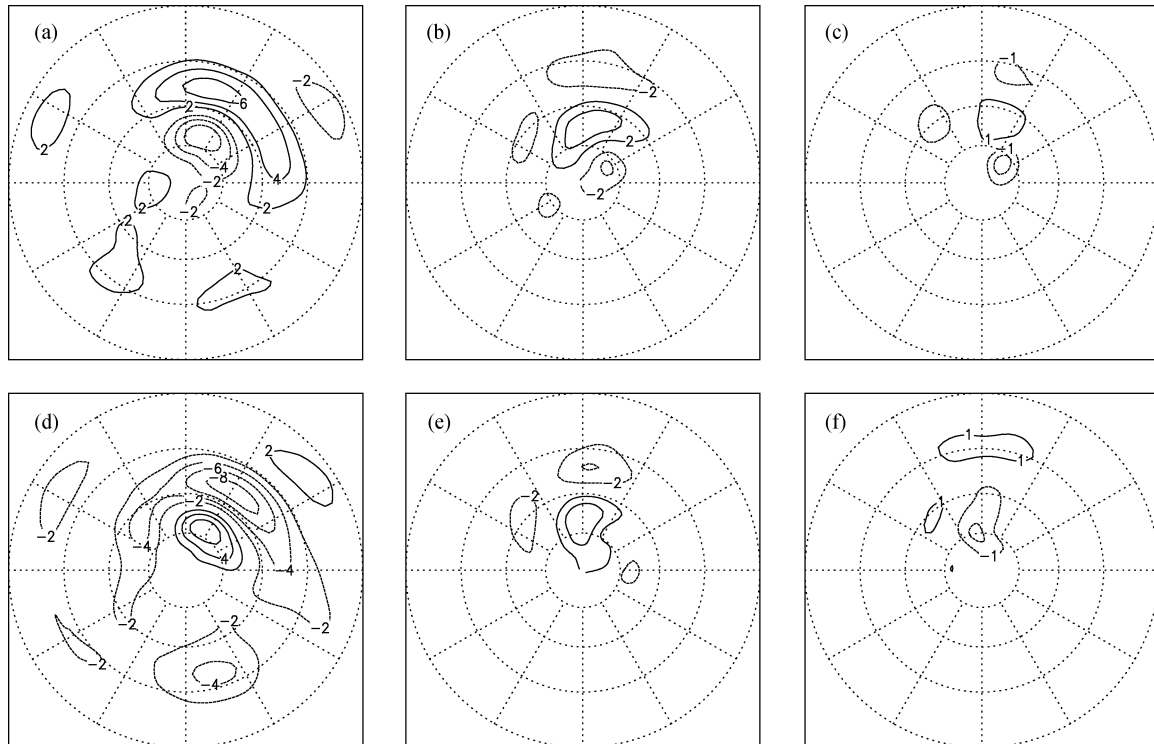
Figure 4 Steady responses. (a) Composite NAO positive phase mode; (b) Difference field between the linear response and the NAO mode; (c) Same as (b), but for the nonlinear response; (d)–(f) Same as (a)–(c), but the composite mode is negative(Units: $10^6 \, \text{m}^2 \, \text{s}^{-2}$).

Table 1 Relative difference between pairs of fields, which correspond to NAO$^{\text{reg}}$, NAO^{+}, and NAO^{-}.

Relative difference	Linear response and NAO mode	Nonlinear response and NAO mode	Linear response and nonlinear response
NAO$^{\text{reg}}$	0.32	0.15	0.27
NAO^{+}	0.71	0.26	0.54
NAO^{-}	0.59	0.22	0.75

(2) The NAO mode has certain nonlinear characteristics. The nonlinear response was more similar to the observed mode than was the linear response. This finding suggests that the nonlinear effect is important in the formation of the NAO.

(3) The effect of nonlinearity is related to the low- frequency anomaly and external forcing. With increasing external forcing and an enhanced low-frequency anomaly, the effect of nonlinearity increased. This finding is supported by the results of ideal experiments and by observed data.

(4) The amplitude of composite NAO modes was larger than that of the regression mode; thus, the nonlinear effect of composite NAO modes is stronger than regression NAO mode. Consequently, nonlinearity should be considered when investigating strong NAO events.

References

Branstator, G., 1992: The maintenance of low-frequency atmospheric anomalies, *J. Atmos. Sci.*, **49**, 1924–1946.

Branstator, G., 1995: Organization of storm track anomalies by recurring low-frequency circulation anomalies, *J. Atmos. Sci.*, **52**, 207–226.

Cai, M., and M. Mak, 1990: Symbolic relation between planetary and synoptic scale waves, *J. Atmos. Sci.*, **47**, 2953–2968.

Fu, C. B., and Z. M. Zeng, 2005: Correlations between North Atlantic Oscillation Index in winter and eastern China Flood/Drought Index in summer in the last 530 years, *Chinese Sci. Bull.*, **50**, 2505–2516.

Hurrell, J. W., Y. Kushnir, G. Ottersen, et al., 2003: An overview of the North Atlantic Oscillation, in: *The North Atlantic Oscillation: Climatic Significance and Environmental Impact*, J. W. Hurrell (Ed), American Geophysical Union, Washington DC, 1–34.

Jin, F. F., and L. Lin, 2007: Closures for ensemble-mean linear dynamics with stochastic basic flows, *J. Atmos. Sci.*, **64**, 497–514.

Jin, F. F., L. L. Pan, and M. Watanabe, 2006a: Dynamics of synoptic eddy and low-frequency flow interaction. Part I: A linear closure, *J. Atmos. Sci.*, **63**, 1677–1694.

Jin, F. F., L. L. Pan, and M. Watanabe, 2006b: Dynamics of synoptic eddy and low-frequency flow interaction. Part II: A theory for low-frequency modes, *J. Atmos. Sci.*, **63**, 1695–1708.

Kalnay, E., M. Kanamitsu, R. Kistler, et al., 1996: The NCEP/ NCAR 40-year reanalysis project, *Bull. Amer. Meteor. Soc.*, **77**, 437–470.

Kug, J. S., and F. F. Jin, 2009: Left-hand rule for synoptic eddy feedback on low-frequency flow, *Geophys. Res. Lett.*, **36**, doi:10. 1029/2008GL036435.

Kug, J. S, F. F. Jin, P. Juhyun, et al., 2009: A general rule for synoptic-eddy feedback onto low-frequency flow, *Climate Dyn.*, **31**, doi:10.1007/s00382-009-0606-8.

Lau, N. C., 1988: Variability of the observed midlatitude storm

tracks in relation to lowfrequency changes in the circulation pattern, *J. Atmos. Sci.*, **45**, 2718–2743.

Li, J. P., and J. X. Wang, 2003a: A new north atlantic oscillation index and its variability, *Adv. Atmos. Sci.*, **20**, 661–676.

Li, J. P., and J. X. Wang, 2003b: A modified zonal index and its physical sense, *Geophys. Res. Lett.*, **30**, doi:10.1029/2003 GL017441.

Murakami, M., 1979: Large-scale aspects of deep convective activity over the GATE area, *Mon. Wea. Rev.*, **107**, 994–1013.

Simmons, A. J., J. M. Wallace, and G. W. Branstator, 1983: Barotropic wave propagation and instability, and atmospheric teleconnection patterns, *J. Atmos. Sci.*, **40**, 1363–1392.

Thompson, D. W., and J. M. Wallace, 1998: The Arctic Oscillation signature in the wintertime geopotential height and temperature fields, *Geophys. Res. Lett.*, **25**, 1297–1300.

Thompson, D. W., and J. M. Wallace, 2000: Annular modes in the extratropical circulation. Part I: Month-to-month variability, *J. Climate*, **13**, 1000–1016.

Walker, G. T., and E. W. Bliss, 1932: World weather V, *Mem. Roy. Meteor. Soc.*, **4**, 53–84.

Wallace, J. M., and D. S. Gutzler, 1981: Teleconnection in the geo-

potential height field during the Northern Hemisphere winter, *Mon. Wea. Rev.*, **109**, 111–125.

Watanabe, M., and T. Nitta, 1998: Relative impact of snow and sea surface temperature anomalies on an extreme phase in the winter atmospheric circulation, *J. Climate*, **11**, 2837–2857.

Watanabe, M., and T. Nitta, 1999: Decadal changes in the atmospheric circulation and associated surface climate variations in the North Hemisphere winter, *J. Climate*, **12**, 494–510.

Wu, B. Y., and R. H. Huang, 1999: Effects of the extremes in the North Atlantic Oscillation on East Asia winter monsoon, *Chinese J. Atmos. Sci.* (in Chinese), **23**(6), 641–651.

Wu, B. Y., R. H. Huang, and D. Y. Gao, 2000: Arctic sea ice bordering on the North Atlantic and inter-annual climate variations, *Chinese Sci. Bull.*, **46**, 162–165.

Wu, Z. W., B. Wang, J. P. Li, et al., 2009: An empirical seasonal prediction model of the East Asian summer monsoon using ENSO and NAO, *J. Geophys. Res.*, **114**, doi:10.1029/2009 JD011733.

Zhou, T. J., X. H. Zhang, Y. Q. Yu, et al., 2000: The North Atlantic Oscillation simulated by versions 2 and 4 of IAP/LASG GOALS Model, *Adv. Atmos. Sci.*, **17**, 601–616.